Military Technical College
Kobry El-Kobbah
Cairo, Egypt

10th International Conference
On Aerospace Sciences&
Aviation Technology

BALLISTIC RESISTANCE OF MODERN LIGHTWEIGHT TARGETS AGAINST THEIR THREAT BY A MEDIUM CALIBER ARMOUR-PIERCING PROJECTILE

BY

A. F. Yakoub[**], A. M. Riad[*], M. K. Shoukry[*] and M. S. Abdel-Kader[@]

ABSTRACT

The continuous development of anti-armor ammunition pays the attention of the designer to construct a new target consisting of lightweight materials such as ceramic and composites. The present work is concerned with the determination of ballistic resistance of ceramic/composite targets; each consists of a ceramic tile backed by a composite with finite thickness. An experimental program has been conducted to manufacture and characterize two types of composites with different thicknesses, respectively. These composites are fiberglass composite (CO) and kevlar-129 composite (K) and they are used to construct five ceramic/fiberglass-composite (Cer/CO) targets and another five ceramic/kevlar-composite (Cer/K) targets. In each constructed target, the thickness of ceramic is constant, whereas the thickness of composite is changed from 2 to 10 mm with 2 mm increment.

The constructed targets are ballistically tested using a medium caliber armor-piercing projectile with an impact velocity of 970 m/s. Due to the projectile impact into the constructed targets, a lot of splinters were produced and it was difficult to measure directly some of the projectile residual velocity using the velocity measuring system. Therefore, steel witness plates were used and the depth of projectile penetration into these plates was measured. A conversion equation, derived from experimental measurements of some residual velocities and numerical results of Autodyn-2D, was used to determine the residual velocity of projectile after perforating each ceramic/composite target. Samples of the obtained experimental results due to the impact of a medium caliber armor-piercing projectile into Cer/CO and Cer/K targets, respectively, are presented and discussed. Moreover, post-firing examinations of tested targets, witness plates and recovered projectiles are photographed for analyzing the test results.

KEY WORDS: Composite mechanics, ceramic/composite armors, impact dynamics, penetration mechanics, and lightweight targets.

** Lecturer, Dpet. of Mech. Engng., A.M.A., Halab, Syria.
* Egyptian Armed Forces
@ Prof. Dr., Dept. of Maritime Engng., Arab Academy for Transporting, Maritime and Technology

INTRODUCTION

Investigating the penetration process through a lightweight armour is necessary for its design optimization. Three main research directions are used for studying the penetration of a lightweight armour by small and medium caliber projectiles. These directions are: (i) experimental, (ii) numerical simulation and (iii) analytical ones. Experimental work could lead to useful empirical relations, e.g. relations between ballistic limit and areal density due to: (a) normal impact of ceramic/metal targets by small caliber projectiles, and (b) oblique impact of such targets by such projectiles [1]. These relations are hardly extrapolated to configure other than those tested. Determination of ballistic efficiency of ceramic, by measuring the depth of penetration into back plate and comparing it with its counterpart into metallic targets, was also tackled [2]. Selecting the most efficient combination of armour components to provide the lightest protection system of ceramic/fiberglass reinforced plastic against any perceived level of threat is another objective of experimentation [3].

Ravid and Bodner [4] investigated analytically the projectile penetration into a ceramic/composite armour. Their model consisted of four stages which were: (i) impact, (ii) penetration in ceramic, (iii) penetration into broken ceramic and penetration in combined (broken ceramic and backup) media, and (iv) backup plate perforation. Stages 1 and 2 were concerned with wave propagation and the projectile penetration through the frontal ceramic layer. Damage of the projectile nose would occur during the initial impact process and broken fragments were ejected. In stage 3, the projectile passed through the fragmented ceramic, which held in place supported by the backing layer and inertia effects. In the fourth stage, the combined fragmented ceramic and the backing layer were considered as a single isotropic plate. They performed a series of ballistic tests on ceramic (Al_2O_3 of 98% purity) bonded to a kevlar backup plate to validate the predictions of their analytical model. The predictions of their model were slightly overestimated the measured ballistic resistance of the ceramic armour systems.

Ravid et. al. [5] extended the work developed by Ravid and Bodner [4] by modifying the final stage of the model to include the deformation and perforation of backup plate instead of perforation only. They modeled the impact of a high-speed projectile into the ceramic backed with kevlar fibers in polymer matrix. Ravid et al. compared the results of their modified model with numerical simulation results. They found that: (i) the backup plates of ceramic tiles provided the support for fragmented ceramic to have effective resistance to ballistic penetration, and (ii) the back plates served to absorb the remaining kinetic energy of the projectile during the final stage of penetration process.

Potti and Sun [6] used a static punch test and the recorded (load-displacement) to capture the highly nonlinear behavior of thick composite laminates during their penetration. They proposed a model for the dynamic penetration process using the data obtained from the static punch curve of a small specimen. The model showed that the delaminated area of the composite target during impact increased when the impact velocity increased until the ballistic limit, beyond which the delamination area decreased with increasing impact velocity.

Straβburger et al. [7] studied the protective strength of high hardness steel /aramid targets. Cylinders of carbon steel were used in order to determine the ballistic effect of natural fragments. The projectile mass was varied in the range from 5 to 53 g and the impact velocity ranged from 400 m/s to 1700 m/s. They found that the increase of the backup plate thickness reduced the behind armor effect and increased the ballistic limit of the targets.

Chocron et al. [8] used the analytical model proposed by Chocron and Sanchez-Galvez [9], to model the penetration process into composite as well as ceramic/composite targets. They showed that the analytical model could be utilized as a design tool to achieve the optimal lightweight armor design capable of defeating the low and medium caliber projectiles. They deduced that the ceramic was effective as a facing material beyond a certain velocity. However, composite configuration was most effective for low impact velocity.

Peskes and Barbero [10] studied numerically the design and optimization of ceramic/composite add-on armor using Autodyn-2D code. They found that: (i) it was more effective to apply high modulii materials instead of high strength materials for backing plates (ii) the projectile deceleration took place in the ceramic for a major part but the additional part performed by composite was relatively low, (iii) the change in the backing layer thickness was less effective than the change in ceramic tile thickness, and (iv) the application of different composite materials as backing plate didn't result in significant differences in the ballistic behavior of the total target.

In the following, five thicknesses of two types of composite have been manufactured; these composites have fiberglass and aramid bases; these are designated by CO and K, respectively. The thickness of each composite are ranged from 2 to 10 mm with increment of 2 mm. The manufactured composites are characterized. Five ceramic/fiberglass-composite (Cer/CO) targets and another five ceramic/kevlar-composite (Cer/K) targets are constructed. The thickness of ceramic in each target is constant, whereas the thicknesses of fiberglass and kevlar composites are changed, respectively. Ballistic tests of constructed targets are perfomed by impacting them with a medium caliber armor-piercing pojectile having a velocity of 970 m/s. The experimental obtained results are presented and discussed. Moreover, photographs of post-firing examinations of each component of target system, recovered projectiles and witness plate are presented.

EXERIMENTAL WORK

In general, the scheme of the experimental work performed included the following phases: (i) Selection of target materials, (ii) material characterization, (iii) target preparation, (iv) ballistic tests and measurements, and (v) post-firing examinations.

Selection of Target Material

Weight represents the key factor to construct a lightweight target. Therefore, ballisticians look for materials having high strengths and low densities rather than steel to construct the lightweight targets. In the present work, both ceramic and composite are chosen as main target materials. The configuration of each constructed target consists of a ceramic tile backed by a composite plate. Ceramic material is selected for the following reasons: (a) it has low density and high compressive strength, and (b) it could be manufactured by different grades and thickness with different mechanical properties, whereas composite is selected because: (a) it has low density and high strength compared with light metal alloy materials, and (b) it is available in local market with different grades, thicknesses and properties. Some of composite materials are easy to be manufactured in laboratory.

Fiberglass fabric was chosen because it had good mechanical properties and the availability of its components in the local market. In addition, kevlar fabric was chosen; it was supplied in the form of sheets with dimensions of 150 mm x 150 mm x 1 mm; each 1 mm-thick kevlar fabric consisted of 4 layers. A steel witness plate was also chosen to determine the depth of projectile penetration inside. The steel plates with dimensions of 150 mm x 150 mm x 13 mm, prepared in MF200 (Military Factory No. 200), were used.

Material Characterization

In the following, the characteristics of projectile, ceramic, and steel witness plate materials are presented, respectively. In addition, the main properties of fiberglass fabric and kevlar fabric, epoxy resin, and fiberglass composite materials necessary for running the analytical model of Ref. [11] were determined, respectively.

Material characterization of projectile, ceramic and steel witness plate

Medium caliber armor-piercing projectiles were used for ballistic testing of ceramic/kevlar-composite and ceramic/fiberglass-composite targets. These projectiles were made of hardened steel. One impact velocity was used for testing the constructed targets. The manufacturer introduced data sheet containing the mechanical properties of projectile material.

The Military Factory No. 200 (MF200) introduced the physical and mechanical properties of ceramic with purity 99%. The steel witness plates were also cut using plasma CNC machine in MF200. Both the chemical composition in weight percent and the mechanical properties of the witness plate material were determined by Moustafa [12].

Characterization of fiberglass fabric

The manufactured fiberglass composite material consists mainly of fiberglass fabric and epoxy resin. The woven-roving fabric was supplied in cloth form, 1.15 m in width and 10 m in length. Mechanical properties in the filling- and warp-yarn directions of this fabric were determined experimentally by Almohandes [13]; these properties are listed in Table 1. There are some mechanical and physical important parameters of fiberglass fabric. These parameters are density, number of yarns per square meter, areal density, and elasticity modulus of fabric as well as cross-sectional area of yarn.

To determine the number of yarns per square meter of fiberglass fabric, ten centimeters of fiber in filling-yarn direction and in warp-yarn direction, respectively, were cut. The number of yarns in each direction was counted. It was found that the number of yarns in filling and warp directions were 45 and 43, respectively. Therefore, the number of yarns per square meter was 880.

The areal density of the fiberglass fabric is represented by the mass of one-meter square of fiberglass sheet. Areal density is one of the most important parameters that characterizes the target and affects the penetration process. For determining the areal density of fiberglass fabric with thickness of 2 mm, ten specimens of woven fiberglass were cut with dimensions 105 mm x 155 mm. Each specimen was weighted individually using a digital balance of 0.0001g accuracy. The mean mass of the ten specimens $\overline{W}$ was determined and the areal density ρ_{ag} is calculated by [14]:

$$\rho_{ag} = \frac{\overline{W}}{A_g}, \qquad (1)$$

where A_g is the surface area of the weighted specimen.

The cross section of fiberglass yarn was determined using both the density and mass of fiber, and equivalent total fiber length per square meter. The following equation is used to determine the cross section area of fiberglass yarn S_g [14]:

$$S_g = \frac{M_{fm}}{\rho_f . L}, \qquad (2)$$

where M_{fm} is the mass of fiber per square meter, ρ_f is the density of fiber and L is the equivalent total length per square meter of fiberglass.

Elasticity modulus of fiberglass fabric can be determined from the recorded load-displacement curve, which was obtained by Almohandes [13]. The strength of fiberglass, σ_{fg} is given by:

$$\sigma_{fg} = \frac{P_{max}}{n_y . S_g}, \qquad (3)$$

Table 1. Tensile test results of fiberglass fabric [13].

Direction	Specimen width, [mm]	Gauge length, [mm]	Elongation [mm]	Breaking strain [%]	Max. load [N]	Breaking strength [N/cm]
Filling-yarn	44	70	3.54	5	2576	585.455
Warp-yarn	44	70	3.54	5	2570	584.091

where P_{max} is the maximum load applied on fiberglass fabric in tensile test, n_y is the number of yarns in tensile test specimen, and S_g is the cross sectional area of a yarn. It was obtained by Almohandes that both the recorded load-displacement curve and the deduced stress-strain curve of the fiber were linear. Therefore, the elasticity modulus represents the slope of stress-strain curve. The elasticity modulus, E, is:

$$E = \frac{\sigma_{fg} . L_o}{\Delta L} , \qquad (4)$$

where L_o and ΔL are the gauge length and maximum elongation in tensile test specimen, respectively.

Characterization of kevlar-129 fabric

In addition to the fiberglass fabric, aramid fabric of type kevlar-129 was also chosen to manufacture another composite for backing the ceramic in the constructed lightweight targets. The delivered kevlar fabric was rolled on carton tubes and wrapped in black shielding protective film. The technical data sheet and the mechanical properties of the chosen fabric are listed in Table 2. Military Factory No. 200 delivers these data. The number of yarn exist under the projectile could be determined from the number of yarns in warp or weft direction. The number of yarn per square meter, n_y, is determined by:

$$n_y = n_{warp} \times \sqrt{2} , \qquad (5)$$

where n_{warp} is number of yarns in warp direction. The calculated number of yarns per meter of the chosen kevlar fabric is 1513 ± 42.

Characterization of Epoxy Resin

The epoxy resin type "Scipoxy Steel" manufactured by the Egyptian company named Master Builders Technologies (MBT) was utilized for preparing the fiberglass composite used in the present work. The epoxy resin was thoroughly mixed with hardener just prior to use. The mass of hardener was one-third of the mass of epoxy. Table 3 lists the main properties of the resin according to the manufacturer specifications.

To determine the tensile properties of the used epoxy resin, four specimens with the 1/3 hardener were initially prepared for testing according to ASTM specifications [15]. The LRX-5K material testing machine was used to carry out the tensile tests for the prepared specimens. This machine has remote control software, which could acquire, record, analyze, store and print the test data [16]. The tensile tests of the prepared specimens were performed in Explosive Department, M.T.C. under the following conditions; crosshead speed of 100 mm/min, gauge length of 60 mm, and maximum load of 5 KN. In addition, both the density and void content of the prepared resin specimens were determined, respectively.

Table 2. Technical data and mechanical properties of kevlar-129 fabric.

Properties		Value
Fiber		kevlar 129, 930 dTex
Warp [yarns/cm]		10.7 ± 0.3
Weft [yarns/cm]		10.7 ± 0.3
Weaving		Plain
Areal density [g/m^2]		200 ± 4% (conditioned)
Thickness [μm]		310 ± 15%
Tensile strength	warp [N/cm]	1400
	weft [N/cm]	1400
Tensile strength in longitudinal direction [MPa]		3380
Elasticity modulus [GPa]		75
Elongation to break [%]		3.4
Density [g/cm^3]		1.44
Decomposition temperature [°C]		~ 500

Table 3. Main properties of epoxy resin type "Scipoxy Steel"

Properties	Data
Color	Gray
Density [g/cm^3]	1.38
Solid content	100%
Pot life	60 min. at 20 °C 30 min. at 40 °C
Curing time	10 hours at 20 °C or 3 hours at 40 °C

Characterization of fiberglass Composite

In the present work, the density of material was determined using its mass in air, W_a, and in water, W_w, and the densities of air, ρ_α (considered to be negligible) and water, ρ_w (1 g/cm^3 at room temperature) [14]. Therefore, the density of fiberglass composite specimen ρ_c is determined using the following equation [14]:

$$\rho_C = \frac{W_a}{\left(\frac{W_a - W_w}{\rho_w}\right)} = \frac{\rho_w W_a}{(W_a - W_w)} . \qquad (6)$$

The volume fraction of fiberglass fabric in a composite is a very important parameter controlling the thermo-mechanical properties of the lamina [14]. There are several methods for determining fiber volume fraction. The method used herein depends on the dissolve the matrix by putting a measured volume of composite specimen, V_c, in an acid. The remained dry fibers after digestion are weighted. Knowing the density of the fibers, the volume fraction of fibers, v_f, is calculated by [17]:

$$v_f = \frac{V_f}{V_C} = \frac{\frac{W_f}{\rho_f}}{V_C} = \frac{W_f}{\rho_f . V_C} , \quad (7)$$

where W_f is the mass of dry fibers.

Polymeric matrix composites typically have voids after fabrication. A well-fabricated composite may have a void content of 1 % or less, whereas a poorly made composite can have a void content as high as 7 % [14]. The void content of a composite can affect its mechanical properties. Thus it is important to know the void content in fiberglass composite and to apply a fabrication method maintaining low void contents. The void content, VO_C, was determined from the measured fiberglass composite density, ρ_c, and the calculated composite density, ρ_t, based upon the known densities of the constituents and the resin content. The calculated density of the composite was represented by the mass, W_C, per volume of composite. The volume of the composite was the sum of the volumes of resin and fibers; these volumes were determined using the known mass of resin, W_r, weight of fiber, W_f, and their respective densities, ρ_r and ρ_f. The density of composite ρ_t is calculated by [14]:

$$\rho_t = \frac{W_C}{V_r + V_f} = \frac{W_C}{\frac{W_r}{\rho_r} + \frac{W_f}{\rho_f}} , \quad (8)$$

where V_r and V_f are the volumes of resin and fibers, respectively. Then, the void content, VO_C (in percent), is calculated by [14]:

$$VO_C = \frac{(\rho_t - \rho_C)}{\rho_t} . 100\% . \quad (9)$$

The standard specimens for tensile testing of fiberglass composite were flat. Tabs were recommended for gripping each specimen. The tabs could be fabricated from a variety of materials including fiberglass, aluminum, or the material being tested [17]. Tabs were bounded to the end of the composite specimen with 2012 araldite adhesive. Four specimens of 2 mm thick were prepared for testing according to ASTM specifications [15]. The tensile test machine using in this test has a maximum load of 15 KN. The other test conditions are similar to that used for tensile tests of resin specimens.

Target Preparation

Fiberglass and kevlar composite plates were fabricated in Explosive Department, M.T.C. The used instruments and the different steps for fabricating these composites are presented in Ref. [11]. Five fiberglass composite plates and another five kevlar composite plates of dimensions 150 mm x 150 mm with thicknesses of 2, 4, 6, 8, and 10 mm were manufactured to be used as backs of ceramic tiles.

The araldite adhesive was used to bond each thickness of the fabricated composites with the ceramic tiles. In addition, the adhesive was used to bond the kevlar fabric sheets until they reached the required thickness. First, the adhesive was prepared according to the manufacturer instructions; it had a pot life of about 20 min. The kevlar fabric layer, cut with dimensions 150 mm x 150 mm, was covered with a thin film of the adhesive, then it was bonded to the second layer and so on. After the adhered layers with required thickness were prepared, they were pressed with ceramic using the hydraulic press for 30 min. under a load of 0.5 ton. Similar load was used for bonding the ceramic and fiberglass composite plates with the required thickness.

In the following, both the kevlar and fiberglass composites are designated by symbols and number. The symbols define the type of material whereas the number defines its thickness. For example, CO2 means fiberglass composite with thickness of 2 mm, whereas K4 means kevlar composite with thickness of 4 mm. In addition, ceramic is designated by Cer.

Ballistic Tests and Measurements

Principle of velocity measurement

The principle of velocity measurement mainly depends on a time measurement of projectile flight over a certain fixed reference base S as shown in Fig. 1. The distance between the two measuring frames, R_{st} and R_{sp}, represents the refrence base; these frames work by infrared photocells. When the projectile passes through the first frame R_{st}, the intensity of the light beam is changed. A start signal is sent to a chronograph, Model INLOC2040, which begins to count the pulses delivered from an oscillator until the gate is closed by a stop signal. The later signal is created when the projectile passes through the second frame R_{sp}. The velocity recorded by the chronograph is the average velocity of the projectile as it passes over the distance S between the two frames and is considered to be the velocity at the midpoint (i.e. at X = B+S/2). The recorded velocity is also displayed on a PC screen.

In the present test, the first frame was placed at 10 m from the muzzle and the second frame was placed at 2 m apart; the midpoint between the two frames was at 11 m from the muzzle. The target mount was placed at 1.5 m from the midpoint between the two frames; i.e. at a distance 12.5 m from the muzzle.

Ballistic setup

The experimental setup was built-up in the Shooting Range of Military Factory No. 45. A scheme of the ballistic setup is shown in Fig. 1. The ballistic setup consists of ballistic barrel, impact and residual velocity sensors Model LS19, target assembly and target mount, velocity measuring devices, and witness plate mount.

Post-firing examinations

These were mainly concerned with the test rig, projectile, target components, and witness plates. After each firing test, the test rig was examined to make sure that all connections were not damaged by the projectile, its fragments or ceramic splinters. The projectiles were recovered and examined in order to study the exhibited type of their failure in addition to the geometry, characteristics of the perforation, and the failure of fiberglass or kevlar composite. All interesting features related to the composite plate deformations and perforations were photographed for analyzing the firing test results.

RESULTS AND DISCUSSIONS

In the following, the experimental results obtained during the course of this work are presented, together with relevant analyses and discussions. These include: (i) characterization results of fiberglass fabric, resin and manufactured fiberglass composite, (ii) ballistic firing test results due to the normal impact of the constructed Cer/CO and Cer/K targets by a medium caliber armor piercing projectile, and (iii) post-firing examinations of the bi-layered tested targets, recovered projectiles and witness plates.

Characterization Results of Fiberglass Fabric, Resin, and Fiberglass Composite

Characterization results of fiberglass fabric

Five specimens of fiberglass yarns were taken for measuring the density of fiberglass fabric. The mass of each specimen in air and in water, W_a and W_w, respectively, were measured and the

density of each specimen was calculated using Eqn. (6). The average density of fiberglass fabric was found to be 2.198 g/cm^3.

Ten specimens were prepared from the original fiberglass fabric sheet as described before. The mass of each specimen was measured. The average mass of the ten specimens was found to be 4.676 g. The areal density of fiberglass fabric was determined using Eqn. (1); it was found to be 287 g/m^2.

Cross section of fiberglass yarn was calculated using Eqn. (2). The measured values of the mass per square meter M_{fm}, fiberglass density and the equivalent total length of 1 square meter of fiberglass were 287 g/m^2, 2.198 g/cm^3 and 880 m, respectively. Thus, the value of the cross-section of the yarn was found to be 0.1484×10^{-6} m^2.

The recorded load-displacement curve obtained by Almohandes [13] was used to determine the value of the maximum load applied on fiberglass during tensile test. In addition, both the dimensions of tensile test specimens and the maximum elongation were considered. The strength and elasticity modulus results of fiberglass in both filling-yarn and warp-yarn directions were calculated using Eqns. (3) and (4). The average values of these parameters were found to be 896.5 MPa and 17.93 GPa, respectively. Moreover, Fig. 2 shows the engineering stress-strain curve of the tested fiberglass fabric.

Characterization results of resin

The density of resin is determined using a similar method for determining the density of fiberglass fabric. Four specimens were prepared. The density of each specimen was calculated using Eqn. (6). The average density of resin was found to be 1.282 g/cm^3.

Voids content of epoxy resin, which was prepared for tensile test specimens, could be calculated using Eqn. (9). Considering the calculated density is 1.38 g/cm^3 according to the manufacture specifications, cf. Table 3, the maximum calculated void content was 7.09%. As mentioned previously, the value of void content must be less than 7%. Therefore, the tensile test specimens of epoxy resin were poorly manufactured. This was due to the experience of the manufacture and the pouring of the specimens under gravity into their specific moulds. Moreover, Fig. 3 shows a typical tensile engineering stress-strain curve for a specimen with 4 mm thickness.

Characterization results of fiberglass composite

The density of fiberglass composite material was calculated for four specimens cut from a thickness of the prepared composites. For each specimen, both the masses in air and in water, respectively, were measured and the density of composite was calculated using Eqn. (6). The values of the measured masses and the corresponding calculated density are listed in Table 4. The obtained results show that all specimens yield extremely close densities indicating the homogeneity of the manufactured composites. The average density of composite is 1.787 g/cm^3.

For each fiberglass composite thickness, the volume fraction was calculated using Eqn. (7). The values of fiber mass, composite volume, and fraction volume of each specimen are listed in Table 5. The recorded results prove the homogeneity of the prepared composites of different thicknesses. Moreover, the average value of fiber volume fraction is found to be 57.4 %.

To calculate the void content, the theoretical density of each thickness of the fiberglass composite was determined. For each composite thickness, both the theoretical density and void content were calculated using Eqns. (8) and (9), respectively. The average values of theoretical density and void content were 1.854 g/cm^3 and 4%, respectively. The values of the void content of the fiberglass composites proved that the prepared composites were well fabricated.

From tensile test of 2 mm-thick fiberglass composite, Figure 4 shows its tensile load-displacement curve. The average value of the elasticity modulus for the fiberglass composite specimens is found to be 10.15 GPa.

Table 4. Masses of each specimen in air and in water, respectively, and the density of fiberglass composite.

Specimen No.	Mass in air, W_a [g]	Mass in water, W_w, [g]	Density, ρ_c [g/cm^3]	Average density, [g/cm^3]
1	0.4837	0.201	1.7110	1.787
2	0.4740	0.215	1.8301	
3	0.4780	0.214	1.8106	
4	0.4990	0.221	1.7950	

Table 5. Values of parameters needed to calculate fiber volume fraction for each composite thickness.

Fiberglass composite design.	Specimen dimensions, [cm x cm]	Fiber mass, W_f [g]	Composite volume, V_c, [cm^3]	Average density of fiber, ρ_f [g/cm^3]	Volume fraction, v_f [%]
CO2	15 x 15	64.575	51.85	2.198	57
CO4		129.15	100.50		58
CO6		193.725	156.24		56
CO8		258.3	203.97		58
CO10		322.875	254.50		58

Ballistic Test Results

Determination of projectile impact velocity

Five medium caliber armor-piercing projectiles were fired. The time of flight over the reference base was measured for each projectile by means of chronograph and PC computer. The velocity of each projectile at the mid point of the reference base (11 m from the muzzle) was determined. The target mount was placed at 12.5 m apart from the muzzle; the projectile velocity at the mid point of reference base was considered to equal the impact velocity. Average impact velocities measured by chronograph and PC were 978.8 m/s and 979.2 m/s and the corresponding percents of error were found to be 1.069% and 1.055%, respectively.

Determination of projectile residual velocity

When the projectile perforated Cer/CO or Cer/K targets, the direct measurement of projectile residual velocity in shooting range of Military Factory No. 45 was very difficult. The projectile velocities after perforating four constructed targets are not recorded by the velocity measuring devices. This was due to the ceramic fragments that spread after striking the tile by projectile, which cut the cables connecting the sensors to the measuring devices. Therefore, it was necessary to look for another method determining the residual projectile velocity in addition to the direct method. The depth of penetration in steel witness plate was used to determine the projectile velocity after perforating each of the remained Cer/CO and Cer/K targets.

During the ballistic tests of the remained Cer/CO and Cer/K targets, the residual velocities were measured directly for projectiles perforating two targets only, whereas the depths of penetration into the witness plates were measured for all projectiles. Each recovered projectile was weighted; the mass of each projectile was found to be close to 85 g. This was attributed to the low impact velocity of projectile so that the projectile was not subjected to erosion when it struck

into the witness plate. In addition, the depth of penetration of each projectile into the witness plate was proportional to its impact velocity. The impact velocity of projectile in witness plate was considered to be equal to the projectile velocity after perforating Cer/CO and/or Cer/K targets.

To determine the residual velocity of projectile, it is necessary to determine the relation between the depth of projectile penetration into the witness plate and the corresponding impact velocity. Two impact velocities of projectile and their corresponding depths of penetration into witness plates were recorded. These data were not enough to predict the required relation. Therefore, a finite difference code, Autodyn-2D, was used to extrapolate the data and to determine the required relation. The input data for the projectile and the witness plate materials, respectively, necessary to run the code are listed in Table 6. In addition, Table 7 lists the values of impact velocity of projectile, measured penetration depth into witness plate and the corresponding predicted depth of penetration using the Autodyn-2D, whereas Fig. 5 plots both the measured and the corresponding predicted depths of penetration, respectively, as function of impact velocity. From the predicted results, the relation between the projectile impact velocity and the depth of penetration into witness plate is represented by:

$$V_i = 23.075\, p + 242.23, \qquad (10)$$

where V_i is impact velocity of the remaining projectile into witness plate in m/s, and p is the measured penetration depth into the witness plate in mm. Equation (10) is also used to determine the projectile velocity after perforating each tested target configuration.

It is clear from Fig. 5 that the relation between depth of penetration and impact velocity is approximately linear. The maximum difference between the measured depth of penetration and that obtained by Autodyn-2D is less than 2%. The measured depths of penetration into witness plate are converted into the corresponding projectile residual velocities using Eqn. (10). Table 8 lists the depth of projectile penetration into witness plate after perforating both the constructed Cer/CO and Cer/K targets, respectively, and the corresponding projectile residual velocities.

Table 9 lists number of layers for both fiberglass and kevlar composites back plates, total target thickness and total areal density of each target configuration. The total areal density AD is calculated for Cer/CO and Cer/K targets, respectively, using the following equations:

$$\begin{aligned} AD_c &= \rho_{cer}\, h_c + \rho_C\, h_{CO} \quad \text{for Cer/CO targets,} \\ AD_k &= \rho_{cer}\, h_c + \rho_k\, h_k \quad \text{for Cer/K targets,} \end{aligned} \qquad (11)$$

where AD_c is areal density of Cer/CO target, AD_k is areal density of Cer/K target, h_{CO} is the thickness of fiberglass-composite plate, ρ_k is the density of kevlar-composite, and h_K is the thickness of kevlar-composite plate.

The ballistic resistance of each tested target is represented by the projectile energy loss during the penetration process. The energy loss, ΔE, is represented by:

$$\Delta E = \frac{1}{2} m_{p_o} V_i^2 - \frac{1}{2} m_r V_r^2, \qquad (12)$$

where m_{po} is the initial mass of the projectile, and m_r is the residual projectile mass. For each target configuration, Table 9 lists the residual velocity using Eqn. (10), the projectile energy loss, and the energy loss ratio.

Table 6. Input data to Autodyn-2D for projectile and witness plate, respectively.

Ser. No.	Parameters	Value	
		Projectile	Witness plate
1	Equation of state	Linear	
2	Strength model	Johnson-Cook	
3	Failure model	None	Bulk-Strain
4	Erosion model	Incremental geometric strain	
5	Reference density [g/cm^3]	7.86	
6	Bulk modulus [KPa]	1.59E+8	
7	Reference temperature [°K]	300	
8	Specific heat (c.v.) [J/kg °K]	4.77E+2	
9	Shear modulus [GPa]	82.2	
10	Yield stress [MPa]	1726	1065
11	Hardening constant [MPa]	140	100
12	Hardening exponent	0.26	
13	Strain rate constant	0.014	
14	Thermal softening exponent	1.03	
15	Melting temperature [°K]	1.57E+3	
16	Ultimate strain	0.07	0.15

Table 7. Data necessary to determine the relation between projectile impact velocity and depth of penetration into witness plate.

Ser. No.	Impact velocity, V_i [m/s]	Measured penetration depth, p [mm]	Predicted penetration depth, P_{pr} [mm]
1	450	-	8.47
1	574	16.12	15.8
2	701	19.45	19.1
3	900	-	28.4

Table 8. Depth of projectile penetration in witness plate and the corresponding residual velocity of projectile after perforating each constructed target.

Ser. No.	Target design..	Measured depth of penetration p [mm]	Measured residual velocity, V_{rexp} [m/s]	Residual velocity, Eqn. (10) V_r [m/s]
1	Cer/CO2	-	-	-
2	Cer/CO4	-	-	-
3	Cer/CO6	17.65	-	650
4	Cer/CO8	16.12	574	615
5	Cer/CO10	15.8	-	607
6	Cer/K2	-	-	-
7	Cer/K4	19.45	701	692
8	Cer/K6	-	-	-
9	Cer/K8	18	-	658
10	Cer/K10	17.4	-	644

Table 9. Measured residual velocity and corresponding projectile energy loss, and energy loss ratio through each tested target.

Target design.	Number of layers, n_y	Total target thickness, H [mm]	Target areal density, AD [kg/m^2]	Residual velocity, V_r [m/s]	Projectile energy loss, ΔE [kJ]	Energy loss ratio, $\Delta E/E_i$ [%]
Cer/CO6	30	26	87.722	650	71.43	79.91
Cer/CO8	40	28	91.296	615	73.31	82.02
Cer/CO10	50	30	94.870	607	73.73	82.49
Cer/K4	16	24	80.2	692	69.03	77.23
Cer/K8	32	28	83.4	658	70.98	79.41
Cer/K10	40	30	85	644	71.76	80.28

Figure 6 depicts the change of residual velocity with total target thickness for both Cer/K and Cer/CO targets, respectively, whereas Fig. 7 depicts the change of residual velocity with the number of layers of back plate for the tested targets. It is clear from both figures that the residual velocity decreases with increasing both the total target thickness and number of layers of back plate, respectively. In general, the velocities of projectile after perforating the Cer/CO targets are smaller than that of projectile perforating the Cer/K targets. This may be attributed to the high value of areal density for CO composite. Moreover, the obtained results show that the ballistic resistance of Cer/CO targets is higher than that of Cer/K targets.

Figures 8 and 9 depict the change of projectile energy loss with total target thickness and number of layers of back plate for both Cer/K and Cer/CO targets, respectively. It is seen from these figures that the energy loss increases with increasing target thickness and number of layers. Moreover, the projectile energy loss in Cer/CO targets is higher than that in the Cer/K targets. Figure 10 shows the change of energy loss with total areal density of the Cer/CO and Cer/K targets, respectively.

Figure 11 depicts the change of projectile energy loss ratio with total target thickness of Cer/CO and Cer/K targets, respectively. It is clear from the figure that the projectile energy loss ratio increases with the increase of total target thickness. However, the increase in projectile energy loss ratio is relatively small with increasing the total thickness of Cer/CO and Cer/K targets, respectively.

Post-Firing Examinations

Fragmentation was always associated with the penetrating ceramic tiles. Each tile was disintegrated into fragments with different sizes. In addition, it was seen that the total ceramic tile was shattered into fragments however; the tile was partially confined at its boundaries by a steel frame having a thickness of 10 mm.

Figures 12a and 12b show photographs of front and back face of the perforated fiberglass composite that backs the ceramic during the penetration process of Cer/CO8 target by the used projectile. It is noticed that the area of affected zone is larger than the cross-sectional area of the projectile; this may be attributed to the bottom size of cone-fractured ceramic, which is formed at the onset of penetration process. In addition, it is seen that there is a shear effect on the composite plate, and a tearing of the composite is propagated from the affected zone. This may be due to the square form of composite plate or its well support. Delamination is also noticed between the fiberglass layers over the main affected zone. Finally, it is deduced that the failure modes in composite plate are: (i) tension in yarns, (ii) shear distributed over circumferential of projectile, and (iii) delamination in fiberglass layers.

Figure 13 shows photographs of front and back face of the perforated kevlar composite plate that backs the ceramic during the penetration process of the used projectile into Cer/K4 target. It is seen that the size of the affected zone is also larger than the cross section of the projectile as in fiberglass composite plate, cf. Fig. 13a. Figure 13b shows the front side of K4 plate; the affected zone has pyramid form of square base, this form is similar to that obtain by Navarro et al. [see Ref. [9]]. Finally, it can deduce that the kevlar plates are failed by tension of yarns; shear effect was not observed.

Two steel plates were used as a witness plate to capture the projectile after perforating Cer/CO and Cer/K target configurations. Each steel plate has a thickness of 13 mm. It was found that the facing witness plates always failed by plugging failure mode. Indentation or partial penetration was associated with the second witness plate. Figures 14a and 14b show the partial penetrations in the second plates of witnesses when the projectiles perforate Cer/K8 and Cer/CO10 targets, respectively. In addition, the sizes of partial penetration depths are different in both targets; this is attributed to the value of impact velocity of the projectile into the witness plate.

Figure 15 shows samples of recovered projectiles; it is clear that they are subjected to erosion during their penetration into different bi-layered target configurations. As seen from this figure, the residual lengths of these projectiles are approximately the same. The masses of recovered projectiles were weighted. Table 10 lists the masses of recovered projectiles. These masses are ranged from 44.69% to 45.03% of the original projectile mass. Therefore, it can be deduced that the effect of both fiberglass and kevlar composite plates on projectile erosion is negligible. The erosion only occurs by ceramic tile, which has the same thickness in all tested target configurations.

Table 10. Remaining masses of the used projectiles after perforating some target configurations.

Target design.	Remaining projectile mass, [g]	Remaining mass ratio, [%]
Cer/K4	84.9072	44.69
Cer/K10	85.5617	45.03
Cer/CO6	85.5364	45.02
Cer/CO8	85.4236	44.96
Cer/CO10	85.5617	45.03

CONCLUSIONS

The main conclusions of the present work are summarized as follows:

- The ballistic resistance of the tested Cer/CO and Cer/K targets is high; they absorb about 80% of the projectile impact energy. Moreover, the ballistic resistance of Cer/CO targets is slightly higher than that of the Cer/K targets with the same total thickness.
- Most of the projectile energy loss is dissipated during its penetration into the ceramic tile. However, the projectile energy loss through fiberglass or kevlar composite plate is small; the maximum amount of energy loss during their perforation doesn't exceed 4% of the total projectile energy loss.
- Ceramic fragmentation is always associated with the penetration of ceramic tiles. Therefore, it is necessary to back the ceramic with kevlar or fiberglass composite to contain most of these fragments.
- The effect of fiberglass and kevlar composite back plates of the constructed targets on the projectile erosion is neglected. Projectiles are subjected to erosion only during their

penetration into ceramic so that the masses of recovered projectiles are approximately the same.

- The failure modes associated with the fiberglass composite back plate are: (i) tension in yarns, (ii) shear over the thickness ahead of projectile, and (iii) delamination in fiberglass layers, whereas the kevlar composite back plate is ruptured due to the tension of the yarns.
- The areal densities of the constructed Cer/CO targets are ranged from 80.57 to 94.87 kg/m^2, whereas the areal densities of the constructed Cer/K targets are ranged from 78.6 to 85 kg/m^2. More ceramic thickness is preferable to completely defeat the used medium caliber AP projectile with impact velocity of 970 m/s.

REFERENCES

1. Sadanandan, S. and Hetherington, J., "Characterization of Ceramic/Steel and Ceramic/Aluminum Armors Subjected to Oblique Impact", Int. J. Impact Engng., Vol. 19, pp. 811-814 (1997).
2. Yazive, D. and Parton, Y., "The Ballistic Efficiency of Thick Alumina Targets Against Long Rod Penetrators", 16th Int. Symp. on Ballistics, Quebec, Canada, 26 – 29 September (1996).
3. Hetherington, J. and Rajagoplans, B., "An Investigation into the Energy Absorbed During Ballistic Perforation of Composite Armours", Int. J. Impact Engng., Vol. 11, No. 1, pp. 33 - 40 (1991).
4. Ravid, M. and Bodner, S. R., "Analytical Investigation of Ceramic Armor with Composite Laminate Backing", 18th Int. Symp. on Ballistics, San Antonio, TX, 15-19 November, (1999).
5. Ravid, M., Bodner, S. R. and Chocron, S. I., "Penetration Analysis of Ceramic Armour with Composite Material Backing", 19th Int. Symp. of Ballistics, Interleken, Switzerland, 7 – 11 May (2001).
6. Potti, S. V. and Sun, C. T., "Prediction of Impact Induced Penetration and Delamination in Thick Composite Laminates", Int. J. Impact Engng., Vol. 19, No. 1, pp. 31-48 (1997).
7. Starβburger, E., Senf, E., Rothenhausler, H., Lexow, B. and Jeanquartier, R., "The Resistance of Steel/Aramid Bi-Layered Armor Against Fragment Impact", 17th Int. Symp. on Ballistic, Midrand, South Africa, 23-27 March (1998).
8. Chocron, I. S., Sanchez-Galvez, V., Diaz-Rubio, F. G., Walker, J. D. and Anderson, C. E., "Analytical Study and Optimization of Ceramic/Composite Armors to a Range of Projectile Threats", 17th Int. Symp. on Ballistics, Midrand, South Africa, 23-27 March (1998).
9. Chocron, I. S. and Sanchez-Galvez, V., "An Analytical Model to Design Ceramic/Composite Armours", 17th Int. Symp. on Ballistics, Midrand, South Africa, 23-27 March, Vol. 3, pp. 327-334 (1998).
10. Peskes, G. J. and Barbero, E., "Optimization of Light Weight Add-on Armour for Infantry Fighting Vehicles", 17th Int. Symp. on Ballistics, Midrand, South Africa, 23-27 March (1998).
11. Yakoub, A. F., "Ballistic Resistance of Modern Armor", Ph.D. Thesis, M.T.C., Cairo (2001).
12. Moustafa, K. M., "Penetration Resistance of Multi-layered Metallic Targets", Ph.D. Thesis, M.T.C., Cairo (2001).
13. Almohandes, A., "Ballistic Resistance of Steel-Fiberglass Reinforced Polyester Laminated Plates", M. Sc. Thesis, Cairo Univ., Cairo (1993).
14. Matthews, F. L. and Rawlings, R. D., "Composite Materials: Engineering and Science", Imperial College, London, Chapman and Hall (1993).
15. ASTM, "Standard Method of Test for Tensile Properties of Oriented Fiber Composites", Part 36, D 3039-74 (1975).
16. LRX/LRX5k, "Materials Testing Machine", User Manual, LLOYD INSTRUMENTS LIMITED (1995).
17. Herakovich, C. T., "Mechanics of Fibrous Composites", John Wiley & Sons, Inc. University of Virginia, New York (1998).

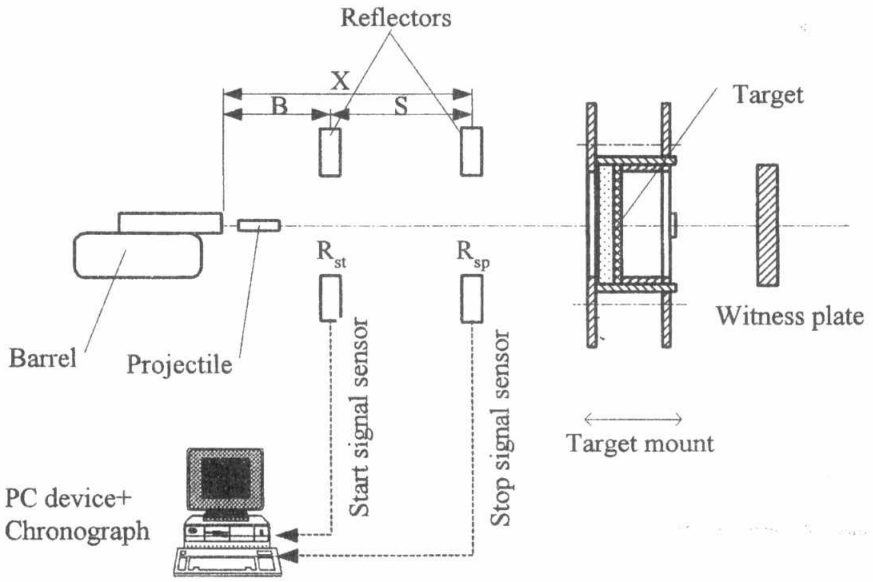

Fig. 1. Scheme of ballistic setup for testing the constructed bi-layered targets.

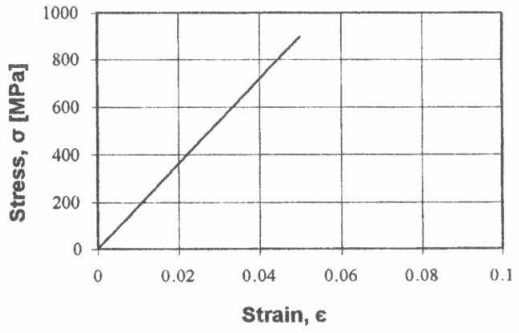

Fig. 2. Engineering stress-strain curve for fiberglass fabric [13].

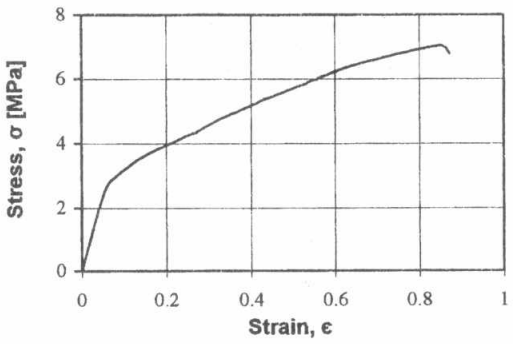

Fig. 3. Typical engineering stress-strain curve for 4 mm-thick epoxy resin specimen.

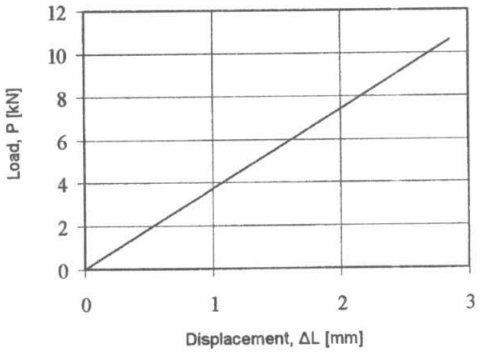

Fig. 4. Load-displacement curve for 2 mm-thick fiberglass composite.

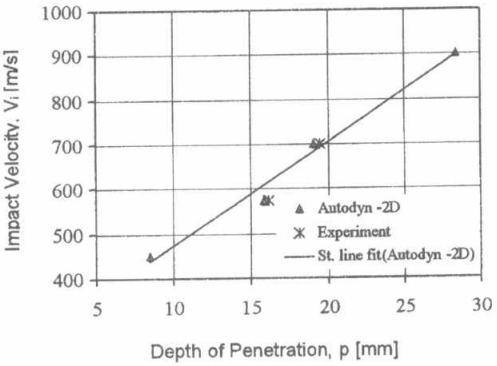

Fig. 5. The change of projectile impact velocity into witness plate with depth of penetration.

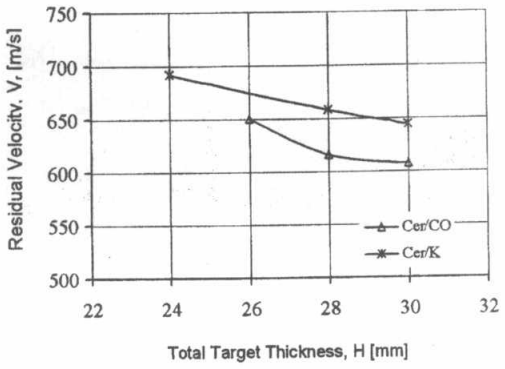

Fig. 6. Residual velocity as function of target thickness for Cer/K and Cer/CO targets, respectively.

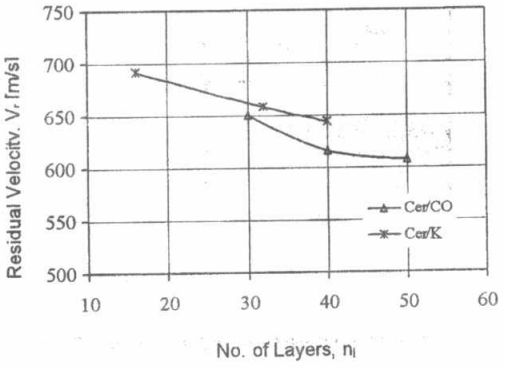

Fig. 7. Residual velocity as function of number of layers for Cer/K and Cer/CO targets, respectively.

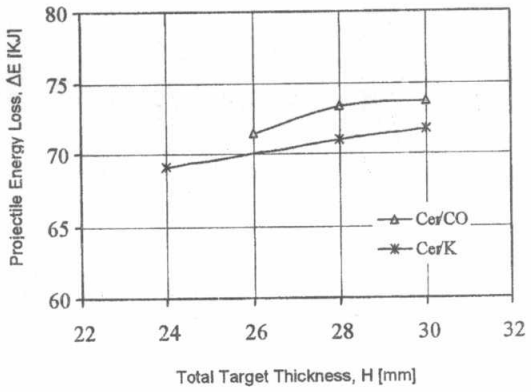

Fig. 8. Projectile Energy Loss as function of total target thickness for Cer/K and Cer/CO targets, respectively.

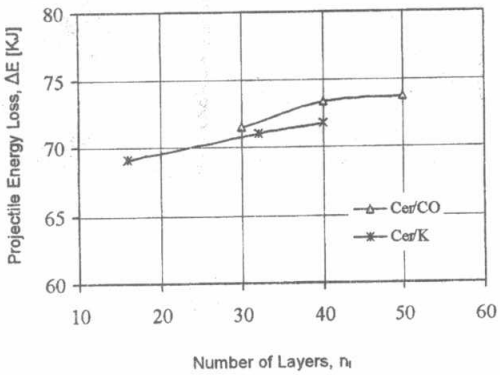

Fig. 9. Projectile energy loss as function of number of layers for Cer/K and Cer/CO targets, respectively.

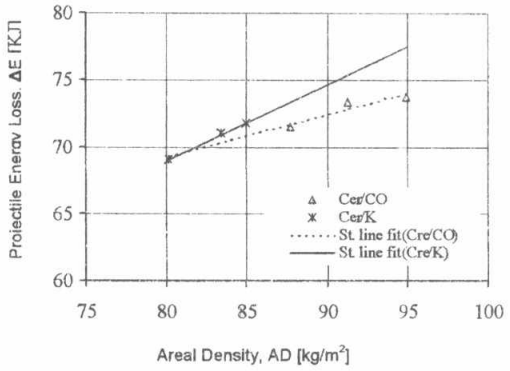

Fig. 10. Projectile Energy Loss as function of areal density of target

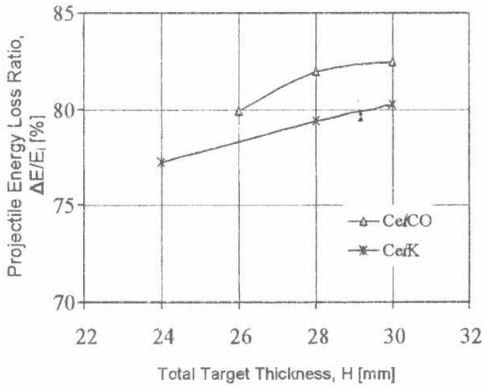

Fig. 11. Projectile energy loss ratio as function of total target thickness.

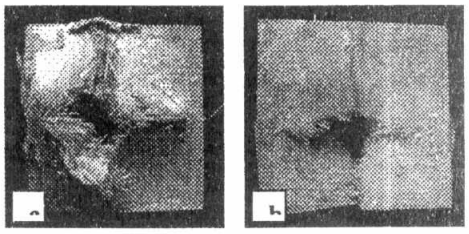

(a) (b)

Fig. 12. (a) Back face, and (b) front of CO8 plate.

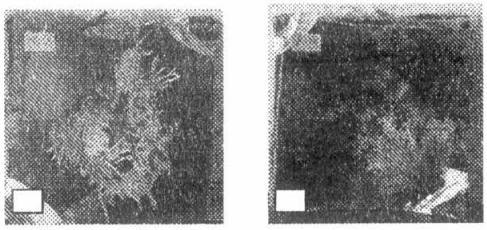

(a) (b)

Fig. 13. (a) Back face and (b) front of K4 plate.

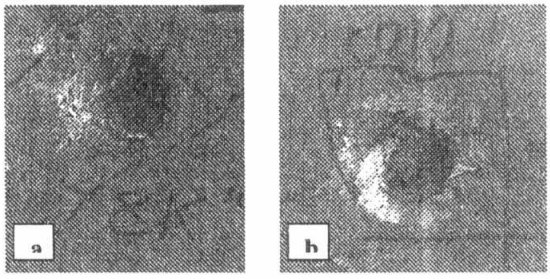

Fig. 14. Partial penetration in second witness plate when the projectile perforates: (a) Cer/K8, and (b) Cer/CO10 targets.

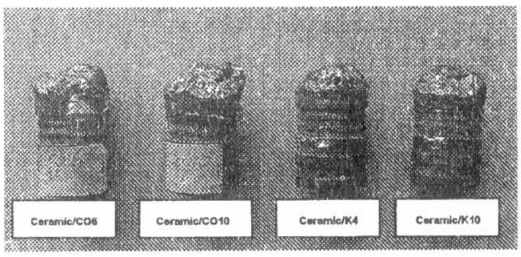

Fig. 15. Recovered projectiles perforating target configurations: Cer/(CO6, CO10, K4 and K10).